ENVIRONMENTAL RESEARCH
LETTERS

LETTER • OPEN ACCESS

Global teleconnections in droughts caused by oceanic and atmospheric circulation patterns

To cite this article: Waqar Ul Hassan and Munir Ahmad Nayak 2021 *Environ. Res. Lett.* **16** 014007

IOP Publishing Environ. Res. Lett. 16 (2021) 014007 https://doi.org/10.1088/1748-9326/abc9e2

ENVIRONMENTAL RESEARCH
LETTERS

OPEN ACCESS

RECEIVED
27 June 2020

REVISED
29 October 2020

ACCEPTED FOR PUBLICATION
12 November 2020

PUBLISHED
18 December 2020

LETTER

Global teleconnections in droughts caused by oceanic and atmospheric circulation patterns

Waqar Ul Hassan and Munir Ahmad Nayak

Discipline of Civil Engineering, Indian Institute of Technology Indore, Simrol, Indore, Madhya Pradesh, India

E-mail: munir_nayak@iiti.ac.in

Keywords: droughts, teleconnections, scPDSI, ENSO

Supplementary material for this article is available online

Abstract

Long-duration droughts are usually tied to persistent local or remote forcings; for example, persistent droughts over California are frequently observed along with the '*ridiculously resilient ridge*' over the West Coast. It is now evident that some oceanic forcings (e.g. El Niño–Southern Oscillation) have *global reaches* and affect multiple regions concurrently during their progression. Here, we show robust significant temporal concordancy of persistent droughts in many regions, revealing multiple teleconnections (distant regions experiencing droughts concurrently), such as the 'Western North America–Mediterranean (WNA–MED)' and the 'Southeast Asia–Southern Africa (SEA–SAF)' teleconnections. Composite pressure and sea surface temperature anomalies during concurrent droughts in WNA and the MED reveal a persistent weather regime that resembles the positive phase of Arctic Oscillation and negative phase of Pacific Decadal Oscillation. During concordant droughts of SEA and SAF, composite pressure anomalies remarkably resemble the El Niño pattern, which we infer as the leading cause of the teleconnection. The insights gained here offer a new dimension to understanding droughts and improving their long-term predictability.

1. Introduction

Droughts are ranked the highest among all-natural hazards, causing substantial damages to humans, the environment, and the economy; take, for example, the recent multi-billion-dollar droughts in California and South Africa (Diffenbaugh *et al* 2015, Lund *et al* 2018, Simpkins 2018, Wolski 2018). Persistent droughts cause devastating damages to humans and the ecosystem health (Yang *et al* 2018b, Xu *et al* 2019), and the losses are likely to amplify in a warmer world (Su *et al* 2018), where the frequency and severity of droughts is expected to intensify (Dai 2011b, Xu *et al* 2019). Discernible changes in droughts and their associated atmospheric patterns have been reported in recent studies (Swain *et al* 2016, Gibson *et al* 2019). Often, atmospheric blocking or anticyclonic circulation (usually a part of quasi-stationary Rossby waves (Nakamura *et al* 1997, Wolf *et al* 2018)) for extended periods results in anomalously dry season in the neighboring regions by preventing moist air from flowing into the region (Wise 2016, García-Herrera *et al* 2019, Gibson *et al* 2019). Such blocking of atmospheric flow and consequent long-duration droughts are most often established and modulated by anomalous sea surface temperatures (SSTs) and teleconnections of remote forcing, e.g. large-scale climatic oscillations (Hoerling and Kumar 2003, Mccabe *et al* 2004, Dai 2011b, Wang *et al* 2014a, Seager and Henderson 2016, Swain *et al* 2017). Studies over Africa, United States, Amazon and Australia (Mccabe *et al* 2004, Ummenhofer *et al* 2009, Lee and Zhang 2011, Masih *et al* 2014, Yang *et al* 2018b) have noted that besides El Niño–Southern Oscillation (ENSO), the dominant mode of global climate variability (Dai 2011b), droughts can be attributed to direct or indirect influence of low-frequency climate variability, such as Pacific Decadal Oscillation (PDO), Atlantic Multidecadal Oscillation (AMO),the Pacific–North America (PNA) pattern, and North Atlantic Oscillation (NAO).

The Pacific SST anomalies modulate and are modulated by anomalies in the Atlantic and the

Indian Oceans at multiple timescales ranging from months to years (Kosaka and Xie 2013, Cai *et al* 2019), and the interactions between the oceanic basins are bound to leave significant footprints in multiple regions simultaneously and sequentially. In fact, a recent study by Boers *et al* (2019) revealed temporal synchronicity of extreme precipitation between multiple distant regions. Synchronous extreme precipitation and other weather extremes of similar characteristics have been reported at regional and global scales (Kripalani and Singh 1993, Hong *et al* 2011, Lau and Kim 2012, Boers *et al* 2019). Studying the role of modes of climate variability on crop production variability, Anderson *et al* (2019) found that the climate modes play a significant role in regional and global crop production variability and may result in globally synchronous crop failure, for example, globally synchronous maize crop failure during 1983 El Niño event. The fact that crop production failure (damage) across the globe is most often associated with the droughts and heatwaves (Lesk *et al* 2016), which are likely to be frequent and intense in future climate (Xu *et al* 2019), raises the concern about international food security under globally synchronous droughts. These observations raise the following critical questions that we answer here, (a) Do we see temporal concordances in droughts over different regions around the globe?, (b) if yes, what are the major driving factors that lead to concordances? and, (c) can they be attributed to oceanic and/or atmospheric climatic oscillations?

Here, we develop a method to quantify temporal concordancy of persistent droughts in different regions, which reveals multiple significant concordant regions. Previous studies have hinted at connections in droughts at regional scales, this study is a unifying step towards identification of teleconnections in droughts among different regions over the globe.

2. Data and methods

2.1. Data

We used high spatial resolution gridded monthly total precipitation (P) and monthly mean temperature (T) from station-interpolated Climate Research Unit (CRU) (Harris *et al* 2020) dataset and two reanalysis datasets, Modern-Era Retrospective analysis for Research and Application, version 2 (MERRA2) (Gelaro *et al* 2017) and European Centre for Medium-Range Weather Forecasts (ECMWF) Re-Analysis fifth-generation (ERA5) (Hersbach 2016) available at spatial resolutions of ($0.5^\circ \times 0.5^\circ$), ($0.5^\circ \times 0.625^\circ$), and ($0.25^\circ \times 0.25^\circ$), respectively. CRU data from January 1901 to December 2017 are used in this analysis. MERRA2 and ERA5 precipitation and temperature data are available from 1980 to the present.

Another important variable for the calculation of the drought index used here is the available water capacity (AWC) of soil, which represents the potential moisture storage capacity of soils and mainly depends on soil texture, among other factors. Here, we used the potential soil moisture storage dataset prepared by Webb *et al* (2000), openly available at NASA's website (https://webmap.ornl.gov/ogc/dataset.jsp?ds_id=548) at $1^\circ \times 1^\circ$ spatial resolution with a downloading option for selecting any different spatial resolution and method of interpolation. The AWC data are downloaded at same grid resolution as that of hydrological datasets using nearest-neighbor interpolation method.

To explore the atmospheric condition causing persistent concordant droughts, we used the average monthly SST, geopotential heights at 200 hPa (Z_{200}) and 500 hPa (Z_{500}) and mean sea level pressure (MSLP) data from ERA5 dataset (Services 2017). We also explored outgoing longwave radiation (OLR) from National Oceanic and Atmospheric Administration (NOAA, Liebmann and Smith (1996)), available at https://psl.noaa.gov/data/gridded/data.interp_OLR.html.

There are various modes of internal climate variability that affect the weather systems at regional or global scales (Lee and Zhang 2011, Vicente-Serrano *et al* 2011, Dai 2011b, Dunn *et al* 2017). These internal modes of climate variability can be either intrinsic to atmosphere, which stem from natural variations in the large-scale atmospheric circulations and are usually linked to blockings, quasi-stationary Rossby waves, and jet streams and have an indirect connection with the tropical SST forcing (Wang *et al* 2014a, Seager and Henderson 2016), or ocean–atmosphere couplings, in which atmospheric circulations are altered by diabatic heating and cooling of atmosphere induced by the large-scale SST anomalies, which in turn influences the SST via several feedback mechanisms (Yang *et al* 2018a). Here, we are interested in understanding the links of concordant droughts with multiple global atmospheric oscillation patterns, such as ENSO, PDO, PNA, Arctic Oscillation (AO), NAO. Many indices are used to quantify the strength of ENSO due to its diverse nature; here we use the Southern Oscillation Index (SOI) to measure the strength and phase of ENSO. Besides that, we tested robustness of our results using SST based indices available at (www.esrl.noaa.gov/psd/gcos_wgsp/Timeseries/). Timeseries of PNA index and other climate indices such as NAO and AO are available at NOAA's Climate Prediction Center (CPC) website www.cpc.ncep.noaa.gov/products/precip/CWlink/daily_ao_index/teleconnections.shtml

2.2. Drought identification

Drought indices are the primary metrics used in identifying droughts and assessing their characteristics. They usually quantify the departure of the available water (e.g. precipitation for

meteorological droughts) from its long-term climatological mean. Among the many drought indices available, the self-calibrated Palmer Drought Severity Index (scPDSI) is most widely used at medium time scales of 9–12 months, e.g. for persistent agricultural drought and moderate hydrological drought (Vicente-Serrano *et al* 2011, Dai 2011a, van der Schrier *et al* 2013). The development of scPDSI resolved most of the shortcomings of the original Palmer Drought Severity Index (PDSI) (Palmer 1965), such as its spatial incomparability and high frequency of extreme events that are actually rare (Alley 1984). Dai (2011a), and many studies have found scPDSI to be a reliable estimator of hydrologic and agricultural droughts. In this study, scPDSI is selected as a measure to detect and quantify droughts.

scPDSI parameters for MERRA2, ERA5 and CRU datasets are calibrated using respective monthly data for the period January 1980–December 2017; due to the availability of longer-length observational data, another calibration period January 1930–December 1990 for CRU was also explored. We defined a region to be in drought for a month when the scPDSI values in at least 25% grid cells in the region are below −2.0 (moderate drought) for that month. Shen *et al* (2007) used 20%, 30% and 40% of grid cells as a spatial threshold to define moderate, severe, and extreme droughts. Aadhar and Mishra (2017) also found that more than 25% of South Asia were under severe to extreme droughts in years 1982, 1987, 1992, 2002, and 2004. Persistent droughts that last for more than 12 months are considered for analyses in this study (Okin *et al* 2018). After finding the persistent drought events, a year is considered a 'drought year' when a minimum of its 6 months are under a persistent drought event (the rest drought months will be in previous or next year).

2.3. Drought probability and significant concordance

The global landmass is divided into 25 reference regions defined in the Fifth Assessment Report (AR5) of the IPCC available at www.ipcc-data.org/guidelines/pages/ar5_regions.html with minor modifications to Western North America (WNA) and Alaska because the 2011–2013 drought in California was not reproducible with these regions (See table S1 and figure S1 for region definition) (available online at stacks.iop.org/ERL/16/014007/mmedia). According to Working Group 1 of the fourth assessment report of IPCC (Trenberth *et al* 2007), the land temperature has increased in recent decades; similar trends are observed in the datasets used here. The annual probability of drought for each region is estimated using equation (1) below. Figures S2–S3 and table S3 show the annual probability of droughts in each region for the datasets used.

$$\hat{p}_i = \frac{n_i}{N} \tag{1}$$

where, n_i = number of drought years in region i, and N = total number of years.

For each pair of regions, temporal concordance analysis is performed as follows. Two regions i and j are said to be under a concordant drought in a year if both the regions are experiencing a drought year simultaneously (e.g. Year 2010 will be a concordant drought year if both i and j are under drought in 2010), and the probability of this happening $\hat{p}_{ij}$, i.e. fraction of years in concordant droughts, can be taken as a measure of concordancy between the two regions. If the regions are independent, the estimated concordance probability is $\hat{p}_i \times \hat{p}_j$. A one-tailed binomial test was carried out at 5% and 10% significance level to test the statistical significance of the large temporal concordance for each pair of regions. The test can be written as:

$$\begin{aligned} H_o &: \hat{p}_{ij} = \hat{p}_i \times \hat{p}_j \\ H_a &: \hat{p}_{ij} > \hat{p}_i \times \hat{p}_j \end{aligned} \tag{2}$$

where, H_o is the null hypothesis that drought in regions i and j are independent or concordancy is same as expected under independence assumption, and H_a is the alternate that the concurrent droughts in the two regions are higher than expected under independence assumption. In our case, we do not need to apply multiple comparison correction, such as field significance, as the null hypothesis does not remain the same when testing different pairs of regions. Robust concordance between two regions is the one that is present in at least two datasets at 10% significance level. Here, we discuss results based on 10% significance, since the reanalysis data is only for 38 years and it is challenging to achieve small p-values with such small sample size.

2.4. Underlying driving factors and connection with climate oscillations

Southeast Asia–Southern Africa (SEA–SAF) and Western North America–Mediterranean (WNA–MED) robust concordances were selected to understand the factors responsible for these persistent concordant droughts. These pairs were selected because of the recent persistent droughts in these regions (Seager *et al* 2015, Hanel *et al* 2018, Wolski 2018) and large distances between the regions, signifying teleconnections in droughts. Standardized precipitation and temperature anomalies during concordant winters were analyzed to evaluate the relative influence of precipitation deficit and warm temperatures on the drought concordances. Composite geopotential height and MSLP anomalies (Z_{200}, Z_{500} for WNA–MED, and Z_{200}, and MSPL for SEA–SAF) for winter months during concordant drought events and 6 months before the concordant drought events

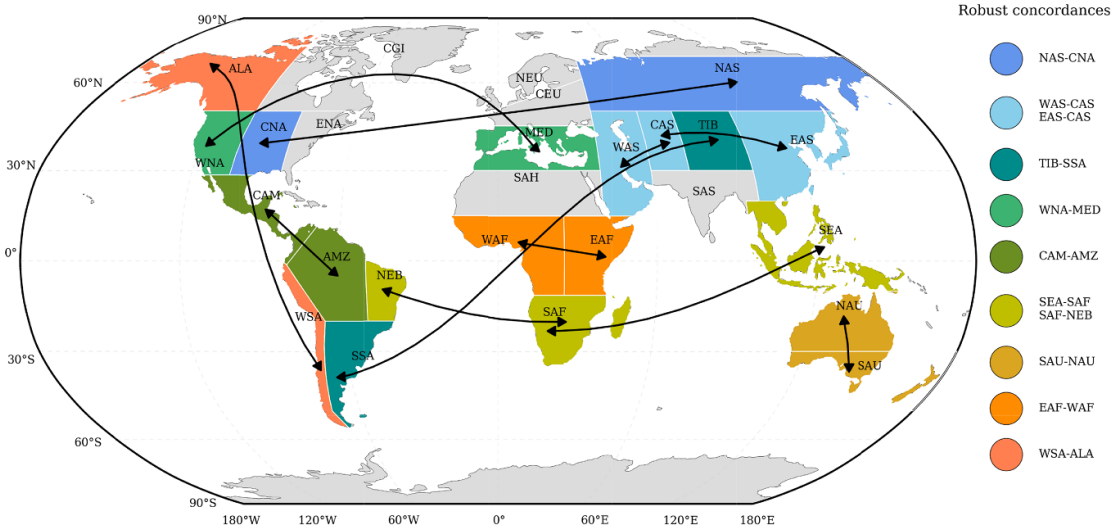

Figure 1. Significant robust concordances identified. Regions with the same color represent robust concordant pairs, while the light-gray colored regions either show zero concordance or concordance is identified in only one dataset.

were analyzed to understand the atmospheric condition leading to concordancy in droughts. Composite SST and OLR anomalies were also explored to gain further insights into the physical factors leading to the two drought concordances (details in supplementary section 2). Winter months were selected for composite anomalies calculation keeping in view the fact that if the rainy season for a region (for example, the winter season for WNA, MED) (figure S4) is dry and under drought, then other months, which usually receive a lesser amount of precipitation, will most likely be under drought. Also, three out of four regions of selected pairs receive most of its precipitation during boreal winters (figures S4–S5) and only 'Southeast Asia' receives precipitation throughout the year.

We analyzed the phase and strength of various climatic modes (atmospheric and oceanic circulation mode) during the concordant droughts to explore their association the concordant droughts. Annual SOI computed by taking the average of monthly values over the year was also explored for SEA–SAF concordancy. A month or a year is said to be in El Niño (La-Niña) phase if monthly or annual SOI is less (greater) than −0.5 (0.5).

3. Major findings

3.1. Probability of droughts

The approach used to identify temporal concordances requires estimation of annual probability of droughts for each region. Since scPDSI is sensitive to precipitation, temperature, and the calibration period (Karl 1986), we first compute the differences in precipitation and temperature among the different hydrologic datasets used here (table S2). These differences in the input datasets and the calibration periods translate to the estimates of annual probabilities and the corresponding temporal concordances (figures S2 and S3). Some regions, such as the Mediterranean, Central Europe, Canada and Greenland, and the Southern Australia have almost similar probabilities in all the four datasets despite the variations in the data (table S3), which can be attributed to similar long-term changes in precipitation and temperature observed in all datasets (table S2). In general, drought probabilities in the recent decades (1980–2017, figure S2) have drastically increased in most regions as compared to the historical period (1901–2017, figure S3) (Trenberth *et al* 2007, Diffenbaugh *et al* 2015, Xu *et al* 2019), with some exceptions such as the Central North America, where megadroughts like dustbowl lasted for 10 years in the 1930s.

3.2. Robust concordances

We present significant robust concordances in figure 1 and tables S4–S5. A total of 17 (7) statistically significant and robust concordances were found at 10% (5%) significance levels. We found that some adjacent regions show robust concordance at 10% significance, for example, 'Northern Australia and Southern Australia', 'North East Brazil and Amazon', 'East Asia and Tibet' and other pairs. As suggested by a few recent studies, such as Herrera-Estrada *et al* (2019) and Miralles *et al* (2019), droughts can self-intensify due to increased sensible heat flux and regulation of atmospheric boundary layer condition via land-feedback mechanism, and they can self-propagate by reduced moisture transport and enhanced heat flux from the upwind drought region. Thus, the concordances observed in adjacent regions can be mainly attributed to self-intensification and self-propagation of drought events. Noteworthy, however, are the significant robust temporal concordances in the region pairs that are distant from

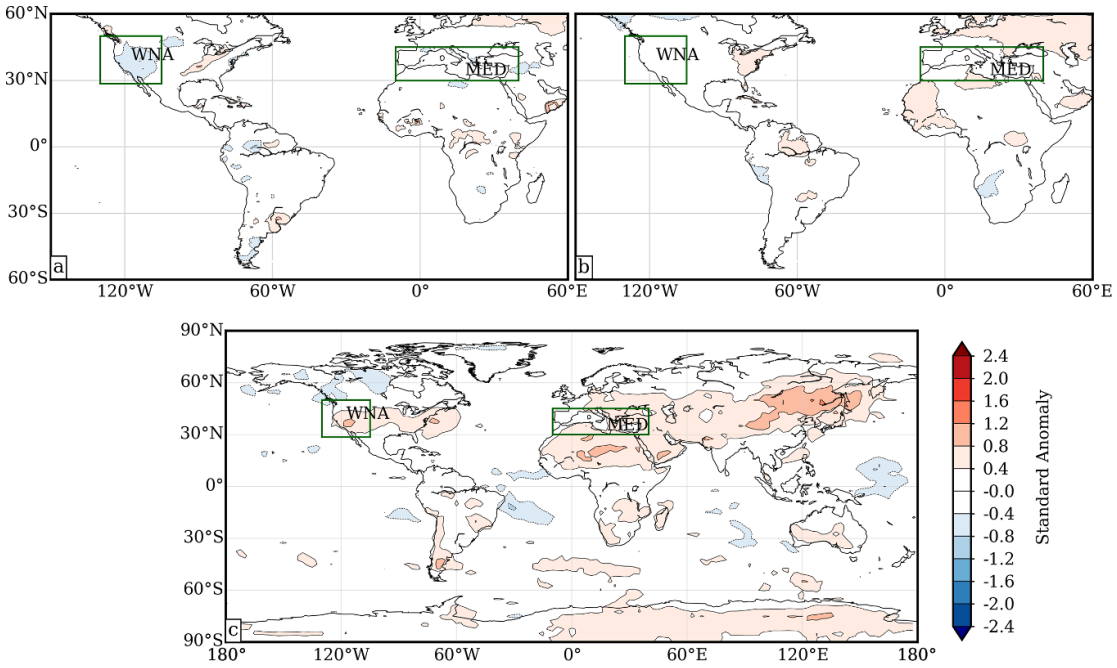

Figure 2. Standardized composite anomaly during the winter concordant months of WNA–MED teleconnection. (a) Precipitation anomalies, (b) temperature anomalies, and (c) OLR anomalies.

each other, on the scale of 10 000 km, for example, 'SEA–SAF', 'WNA–MED', and others (table S5). We call these concordances '*teleconnections in droughts*'. Region pairs 'Central Asia–Western Asia' and 'Eastern Africa–Western Africa' bear significant concordance in almost all datasets regardless of variations among them, signifying strong temporal interaction of droughts between the regions.

Though our focus here is on significant and robust concordances, we note that some region pairs also show significant concordances individually in different datasets (tables S4–S5) and should be examined in detail in future studies.

3.3. Underlying driving factors and connection with climate oscillations

To explore the major driving factors, in terms of atmospheric and oceanic patterns, and to corroborate the teleconnections revealed in the previous section, we further analyzed two robust significant concordant pairs, 'WNA–MED' and 'SEA–SAF'. These two pairs were selected because the regions there are distant and WNA and SAF endured persistent severe droughts recently (Lund *et al* 2018, Wolski 2018). For WNA–MED robust pair, winter standardized precipitation and temperature anomalies are shown in figure 2. From these, we observe that precipitation, as well as OLR in both regions, is roughly one standard deviation below average; whereas the temperatures in both are near normal. This suggests that the major factor for WNA–MED concordance is the deficit in precipitation. We observe a zonal band of suppressed convection over northern mid-latitudes centered over Western US and Eastern Russia, which indicates a northward shifting of the jet stream during the teleconnection.

For SEA–SAF pair, both precipitation deficits and warmer temperature seem to contribute in driving the teleconnection (figure 3). In has been suggested that precipitation deficits normally initiate droughts and higher temperatures tend to intensify them (Hanel *et al* 2018, Luo *et al* 2017). OLR anomalies during the concordant winter months also suggest lack of cloud cover and suppressed convection over both regions. However, the pattern of deep convection in central Pacific Ocean and suppressed convection in its western pool suggests that the teleconnections in SEA–SAF droughts happens during El Niño periods. We also observe suppressed convection over west coast of equatorial South America and Northern Brazil that may have resulted from the descending branch of the Walker Circulation during El Niño events (Hill *et al* 2009). In addition, enhanced deep convection is noted over south of Northern America and subtropical southern America, which is often linked with El Niño via quasi-stationary Rossby wave train (Hill *et al* 2009, Bruick *et al* 2019).

A peculiar pressure pattern is observed in upper atmospheric levels (at 200 hPa) during winter months of WNA–MED concordant droughts (figure 4). Height anomalies at 500 hPa also conspicuously depict a similar pressure pattern (figure S6). The persistent ridges over North Pacific and Eastern Europe are often associated with the low-frequency planetary waves (Wang *et al* 2014a, Kornhuber *et al* 2019), fueled by the eddy transport of momentum and enthalpy over North Pacific and North Atlantic ocean (Nakamura *et al* 1997), respectively. These

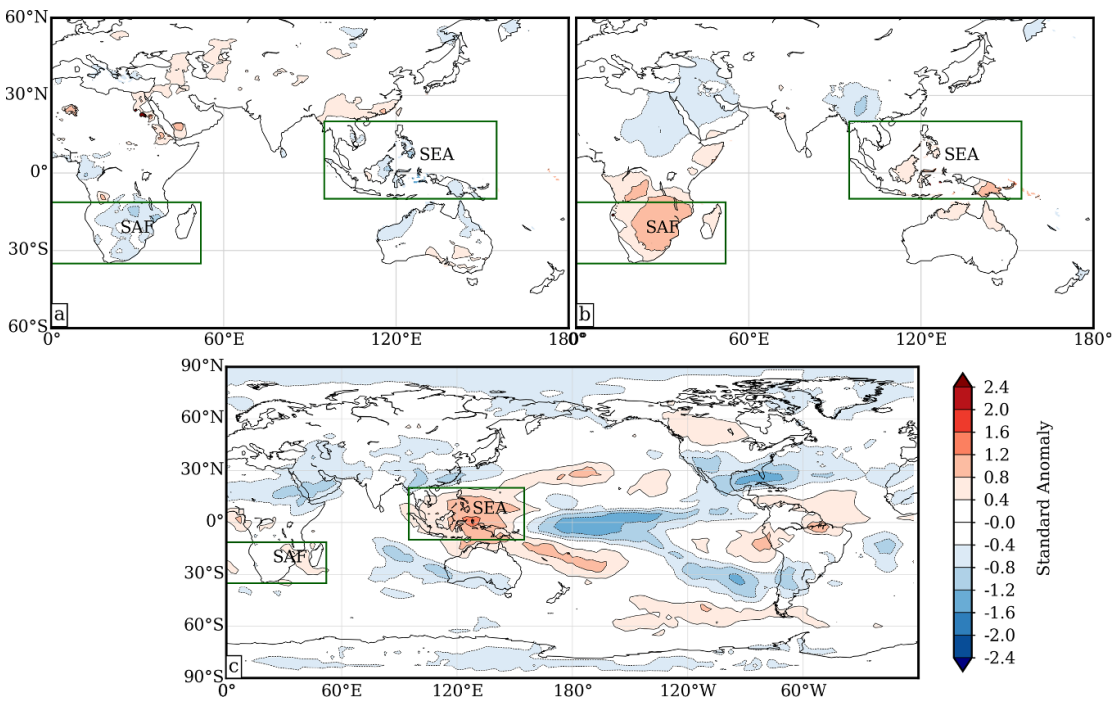

Figure 3. Same as figure 2, but for SEA–SAF pair.

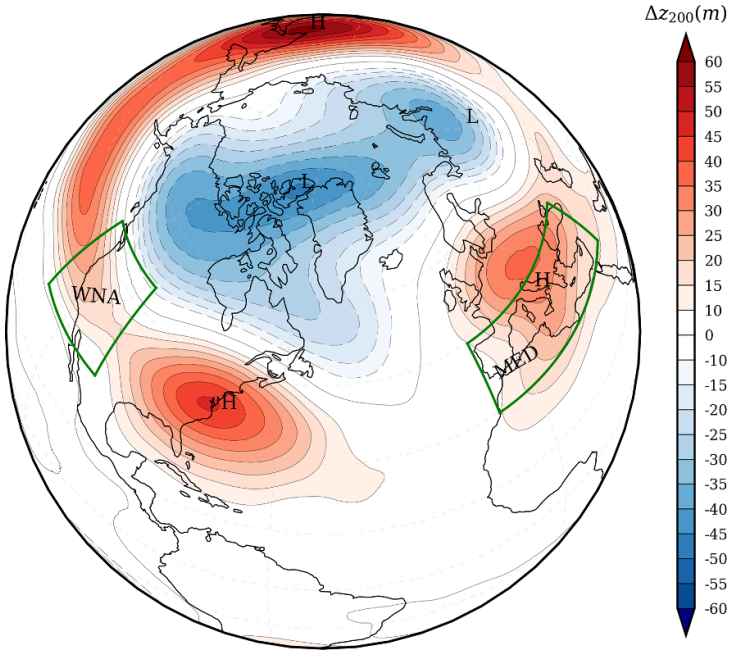

Figure 4. Composite anomalies of geopotential heights at 200 hPa level during winter concordant months for WNA–MED teleconnections. Shading/contours represent composite pressure anomalies, where red shades (blue)/solid lines (dashed) correspond to above (below) normal heights. A similar figure but on cylindrical map projection is given in figure S16.

high-pressure systems divert and/or disrupt storm tracks and block moist air from flowing into WNA and MED (Seager *et al* 2015, Hanel *et al* 2018, García-Herrera *et al* 2019, Gibson *et al* 2019), resulting in below-normal precipitation and above-normal temperatures in both regions and lead to concordant droughts. Several studies have highlighted the role of tropical SST variability (such as ENSO) in the development and maintenance of the high-pressure blocking (Wang *et al* 2014a , Swain *et al* 2017, Seager and Henderson 2016). Composite height anomalies (Z_{200hPa} and Z_{500hPa}) 6 months before concordant droughts also depict mild high-pressure systems near the west coast of WNA and over MED favoring onset of persistent droughts in both regions (Seager *et al* 2015, Hanel *et al* 2018),

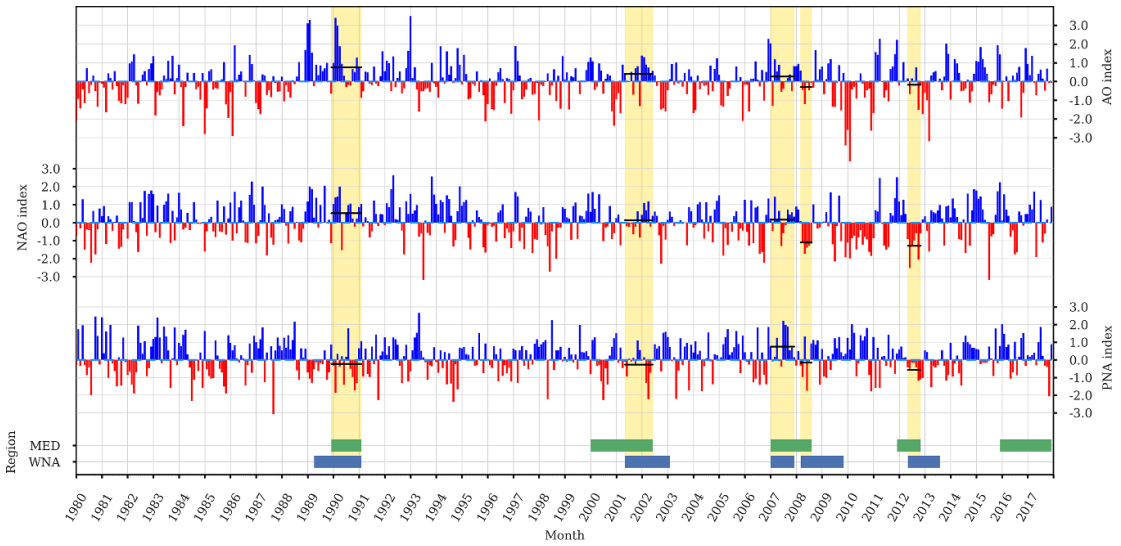

Figure 5. Atmospheric teleconnection patterns AO, PNA and NAO during WNA–MED concordant droughts. About 60% (55%) of total concurrent drought months (golden column) have occurred during positive phase of AO and NAO and negative phase of PNA (red and blue bar series, red bars represent negative index value, blue bars represent positive index value). Blue and green horizontal bars represent persistent droughts over Western North America and Mediterranean regions, respectively. For winter concordant month see figure S8.

which later translate to concordant drought periods (figure S7).

Height anomalies presented above resemble strongly with positive phase of the AO (AO+,), positive phase of the NAO (NAO+, a close akin of AO+ but local to Atlantic ocean (Ambaum *et al* 2001)), and negative phase of the PNA teleconnection pattern (PNA−, Wallace and Gutzler (1981)). About 60% of concordant periods are in positive phase of AO and, as expected, a similar fraction of winters is in positive phase of NAO. In addition, PNA− is observed in ~60% of the concordant drought months (figure 5). If we consider only the concordant winters, about 70% fall in AO+ and ~50% in negative PNA− (figure S8). Furthermore, the SST anomalies are persistently negative near the west coast of US and the eastern equatorial Pacific Ocean, signifying a negative PDO and near-normal phase of ENSO (Mccabe *et al* 2004); offshore cold waters lead to reduced inland moisture transport from oceanic basins and tend to favor drought conditions (figure S9). In addition, composite SST anomalies in Atlantic basin remarkably resemble with the positive phase of AMO. About 87% (~67%) of winter concordant months are observed during PDO− and AMO+ (figure S10). On exploring the role of ENSO in WNA–MED, we note that about ~70% of concordant winter periods occur when ENSO is in its normal phase and remaining have a tendency to occur during weak La Niña (figure S11). From figure 2, we observe mild convection in the Pacific Ocean near western pool suggesting the normal phase of ENSO and non-significant role of ENSO in WNA–MED teleconnection. These results suggest that AO+, PDO− and PNA− play a significant role in causing WNA–MED drought teleconnections. It is clear then that a coupling of multiple atmospheric patterns may explain all concordant droughts in WNA–MED, a concept similar to *weather regimes* (Baldwin and Dunkerton 2001), such as the *Western Hemisphere circulation* as an association of ridge over North Atlantic and Northeast Pacific resembling NAO+ and PNA+ (Tan *et al* 2017).

Figure 6 shows the composite boreal winter anomalies of 200 hPa geopotential heights during the concordant drought events for SEA–SAF robust pair. This pattern remarkably resembles the warm phase ENSO, i.e. El Niño. The anticyclonic conditions persisting over S. E. Asia and twin cyclones over Southern China and the Western Australia (Adames and Wallace 2017) divert upper-level winds towards the cyclonic centers and generate easterlies in lower layers (figure S12), which manifests in weakening of the Walker circulation, leading to precipitation deficits over S. E. Asia (Ropelewski and Folland 2000, Hendon 2003). The localized high-pressure ridge near and over South Africa with anticyclonic flow and decreased strength of *Angola low* (figure S12) hinder the moisture inflow from southwest Indian Ocean and Southeast Atlantic ocean resulting in drying of South Africa (Munday and Washington 2017, Pomposi *et al* 2018). Composite MSLP anomalies during the boreal winter months of concordant droughts again conform to El Niño signature. Persistent warm anomalies in the central/eastern Pacific and cold anomalies in western pool during the winter concordant months (figure S13) also suggest El Niño as the major cause for SEA–SAF droughts teleconnections. Furthermore, SST anomalies near the west coast of North America are higher than the normal,

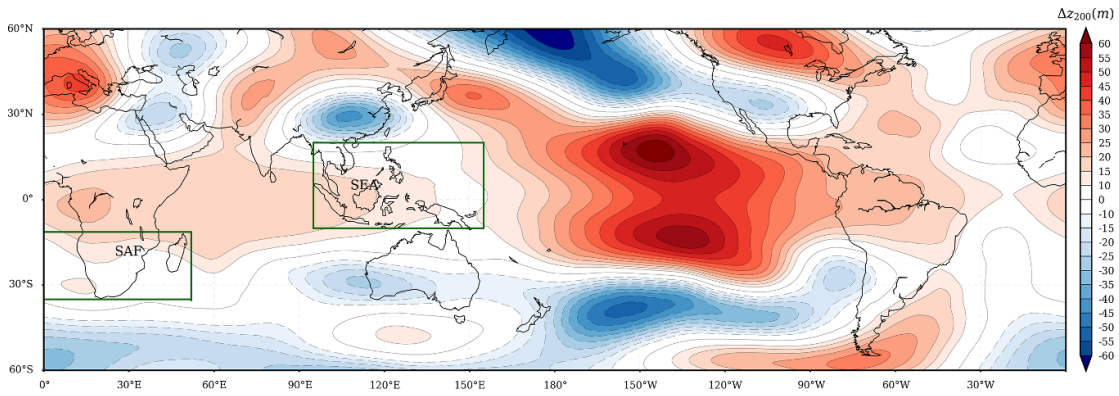

Figure 6. Composite anomalies of geopotential heights at 200 hPa level during winter concordant months for SEA–SAF teleconnections. Shading/contours represent composite pressure anomalies, where red shades (blue)/solid lines (dashed) correspond to above (below) normal heights. A similar figure but for the whole globe is given in figure S16 for comparison with composite height of WNA–MED pair.

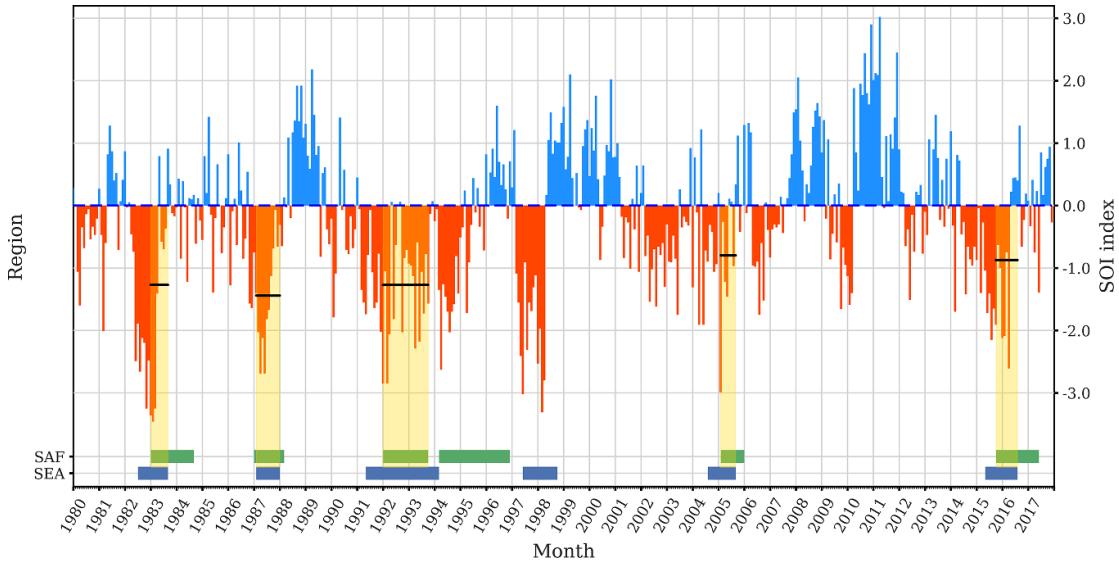

Figure 7. Relationship of SEA–SAF concordant drought events with warm phase of ENSO. All temporally concurrent drought months (golden column) have occurred during negative SOI (red and blue bar series, red bars represent negative SOI, blue bars represent positive SOI), which represents warm phase of ENSO (i.e. El Niño). Blue and green horizontal bars represent persistent droughts over Southeast Asia and South Africa regions, respectively. Similar plot at annual time scale is given in figure S17.

which suggests that positive PDO may have some contribution in causing the teleconnections.

For validation, we examined the strength and phase of ENSO events during the concordant drought events in figure 7, which shows the timeseries of SOI (the atmospheric counterpart of SST based El Niño) and drought periods in the two regions. All concurrent drought events are observed in the second half of the El Niño phase of ENSO with an average strength of SOI as −0.8, characterizing a moderate to extreme El Niño. Besides the conventional well-known El Niño (positive SST anomaly in the Eastern/Central Pacific), Kao and Yu (2009) and Ashok *et al* (2007) have recognized another type of El Niño that has strong positive SST anomalies in the central Pacific, known as 'El Niño Modoki'. These studies showed that the two differ in spatial pattern, formation mechanism, and their influences on global climate. On comparing SST anomalies of SEA–SAF pair and the four dominant EOF modes of SST anomalies in tropical Pacific defined by Ashok *et al* (2007) (see figure 2 of reference), we found that SST anomalies during SEA–SAF concordancy (figure 6) show remarkable resemblance with the first leading mode of SST anomalies, which they call the conventional well-known El Niño. To assess the robustness of our results to ENSO indices, we analyzed multiple SST based indicators of ENSO during SEA–SAF concordancy and found that all concordant droughts have occurred in El Niño phase of ENSO (figure S14). Consistent with the results from SOI index, SST based ENSO indices also highlight the occurrence of concordant drought in the second half of strong El Niño events. Similar results were obtained with annual SOI, where all concordant

droughts are observed to occur during El Niño events. Many studies such as Wang *et al* (2008) and Dong *et al* (2018) have noted that ENSO impact on climate is not stable and is modulated by PDO. They suggested to consider the phase of PDO when using ENSO as a predictor in forecasting. We explored the phase of PDO during the SEA–SAF concordant winters and observed that all concordant winters occur in positive phase of PDO (figure S15), which modulates the El Niño impacts on SEA–SAF teleconnection by amplifying the strength of high pressure over South Africa and southern Indian Ocean, which in turn inhibits convection and rainfall (Wang *et al* 2014b). In addition, an increased low-level (upper-level) convergence (divergence) in the central pacific during in phase PDO and El Niño (i.e. PDO+ during El Niño) manifests increased convection and enhanced ascending branch of Walker Circulation that tends to strength the atmospheric response and teleconnections of El Niño (Wang and Liu 2016). No concordant drought is observed when PDO was out of phase with El Niño (i.e. PDO+/PDO− during La Niña or PDO− during El Niño); however, concordant droughts tend to terminate when PDO is out of phase (figure not shown). Consistent with the findings of Wang *et al* (2014b) and Nguyen *et al* (2020), we observed increased likelihood of concordant drought conditions in SAF and SEA during PDO+ and El Niño in comparison with El Niño only. Out of five concordant droughts, four have delayed onset in South Africa as compared to S. E. Asia by about 6 months (figure 7), suggesting a delayed response of South Africa to El Niño, though seasonality in precipitation and other local to global factors may also be responsible (Florenchie *et al* 2003, Masih *et al* 2014). From these results, we infer that SEA–SAF teleconnection is mainly regulated by ENSO and the relationship is modulated by PDO.

4. Discussion and conclusions

We observed that during the historical period 1901–2017 of CRU (under calibration 1930–1990), the annual probabilities of droughts are small about '0.096' on an average as compared to the recent decades 1980–2017 (under calibration 1930–1990), where the average probability has drastically increased to '0.141', likely in response to the pronounced drier and hotter climate in response to the global climatic change. The remarkable shift in annual drought probabilities in many regions is alarming and is supported by recent findings over California and South Africa (Swain *et al* 2016, Simpkins 2018).

Precipitation deficit seemed as the main factor in the drought teleconnections of WNA–MED pair; however, we note that temperature is also important in intensifying droughts and its role is more complex, especially in snow-covered regions like WNA and Europe (Luo *et al* 2017). We observed a zonally symmetric height anomaly pattern during the concordant events of WNA–MED pair (figure 4 and figure S16) that suggests poleward shift of the winter jet stream and storm track from their normal positions. A stronger low-pressure system over the Arctic (polar vortex) and the northward shifting of jet stream (figure 4) during WNA–MED concordance, which are characteristic features of positive phase of AO, result in hot and dry conditions in the Western North America, the Mediterrenean, and some other mid-latitudinal regions. Consistent with the positive phase of AO, a positive NAO pattern is also observed but is local to the Atlantic basin and Europe. The ridiculously resilient ridge during WNA–MED concordance, a dominant cause of droughts in WNA, forms an indispensable component of the pressure pattern that remarkably resembles the negative PNA pattern. Negative phase of PDO during WNA–MED concordance suggests that off-coast cold waters near the west coast of United States may also contribute in causing precipitation deficits over WNA (Mccabe *et al* 2004, Wang *et al* 2014a) and in increasing the concordance likelihood in WNA–MED pair. Overall, a weather regime manifesting as a coupling of mainly AO+, NAO+, PNA−, and PDO− is hypothesized as the dominant mode of oceanic and atmospheric variability responsible for WNA–MED teleconnection.

We identified a persistent high-pressure system over the tropical Pacific Ocean and twin cyclones over China and Australia during SEA–SAF concordances that results in the weakening of Walker Circulation and precipitation deficits over Southeast Asia. The pressure pattern shows a remarkable resemblance with El Niño phase of ENSO, which is further confirmed by OLR and SST anomaly patterns. Positive SSTs (warm waters) near west coast of US during concordance periods feature positive PDO as a decadal modulator of SEA–SAF teleconnection. Consistent with the findings of Ropelewski and Folland (2000), Vicente-Serrano *et al* (2011), we found 80% of the concordant months in SEA–SAF pair during El Niño, suggesting a strong relationship between the SEA–SAF teleconnection and El Niño. This relationship, however, is strongly dependent on the phase of PDO. We observed all concordant droughts when PDO was in phase with El Niño (i.e. PDO+ during El Niño), whereas no concordant drought was noted when PDO was out of phase with El Niño. However, concordant droughts in SEA–SAF pair tend to terminate when PDO is out of phase with El Niño (figure not shown). The strengthening (weakening) of El Niño impacts on SEA–SAF concordancy during PDO+ (PDO−) is consistent with the results of a few recent studies, such as Dong and Dai (2015), Nguyen *et al* (2020), Wang *et al* (2014b). The intensification of Walker Circulation in the central Pacific by PDO+ tends to strengthen the teleconnections of El

Niño, which results in increased high pressure over South Africa, Southern Indian Ocean, and Western Pool of Pacific Ocean, and therefore, inhibits convection and rainfall over the regions (Wang *et al* 2014b, Nguyen *et al* 2020). Though all concordant droughts here can be explained by El Niño dynamics alone, ignoring the phase of PDO may result in inaccurate estimation/prediction of future concordant droughts in SEA–SAF pair. Besides climatic oscillations and SST, other phenomena such as land-atmosphere feedback mechanisms, moisture transport and others may also lead to concordant droughts, (Masih *et al* 2014, Herrera-Estrada *et al* 2019, Miralles *et al* 2019).

An implicit assumption in our analysis of concordancy estimation and significance tests is that annual droughts are independent events, which in some cases may not be valid since multi-year droughts are not uncommon in many regions. The seasonal variability in precipitation may affect concordant drought frequency estimation. Here, we only analyzed droughts that last more than 12 months to account for the creeping nature of droughts and administer to seasonality of precipitation.

Notwithstanding these limitations, we believe that the results presented here provide strong evidence of global teleconnections in droughts, their major driving factors, and their relationship with long-wave climatic oscillations. Our study complements the work on 'teleconnections in extreme precipitation events' and 'globally synchronous crop failure' reported recently.

We stress that though major physical insights into the causes of teleconnections are given in this study, in-depth analysis on causal mechanisms is beyond the scope, and it is imperative to understand the physical processes underlying the observed concordances, their representation in global circulation models, and their impact on the global crop production and food security.

Data availability statement

The data that support the findings of this study are openly available at the following URL/DOI: https://crudata.uea.ac.uk/cru/data/hrg/cru_ts_4.02/ (Harris et al 2020) .

Acknowledgments

The authors would like to thank the three anonymous reviewers whose comments and suggestions have greatly improved the quality of the paper. We also acknowledge and thank the organizations for keeping the data openly accessible, without which the study would not have been possible. The authors would also like to acknowledge the high-performance computing facility provided by Indian Institute of Technology, Indore.

Conflict of interest

The authors declare no competing interests.

ORCID iD

Munir Ahmad Nayak https://orcid.org/0000-0003-2764-3623

References

Aadhar S and Mishra V 2017 High-resolution near real-time drought monitoring in South Asia *Sci. Data* **4** 170145
Adames Á F and Wallace J M 2017 On the tropical atmospheric signature of El Niño *J. Atmos. Sci.* **74** 1923–39
Alley W M 1984 The Palmer Drought Severity Index: limitations and assumptions *J. Clim. Appl. Meteorol.* **23** 1100–9
Ambaum M H, Hoskins B J and Stephenson D B 2001 Arctic oscillation or North Atlantic oscillation? *J. Clim.* **14** 3495–507
Anderson W, Seager R, Baethgen W, Cane M and You L 2019 Synchronous crop failures and climate-forced production variability *Sci. Adv.* **5** eaaw1976
Ashok K, Behera S K, Rao S A, Weng H and Yamagata T 2007 El Niño Modoki and its possible teleconnection *J. Geophys. Res. Oceans* **112** C11007
Baldwin M P and Dunkerton T J 2001 Stratospheric harbingers of anomalous weather regimes *Science* **294** 581–4
Boers N, Goswami B, Rheinwalt A, Bookhagen B, Hoskins B and Kurths J 2019 Complex networks reveal global pattern of extreme-rainfall teleconnections *Nature* **566** 373–7
Bruick Z S, Rasmussen K L, Rowe A K and Mcmurdie L A 2019 Characteristics of intense convection in subtropical South America as influenced by El Niño–Southern Oscillation *Mon. Weather Rev.* **147** 1947–66
Cai W, Wu L, Lengaigne M, Li T, Mcgregor S, Kug J-S, Yu J-Y, Stuecker M F, Santoso A and Li X 2019 Pantropical climate interactions *Science* **363** eaav4236
Dai A 2011a Characteristics and trends in various forms of the Palmer Drought Severity Index during 1900–2008 *J. Geophys. Res. Atmos.* **116** D12115
Dai A 2011b Drought under global warming: a review *Wiley Interdiscip. Rev. Clim. Change* **2** 45–65
Diffenbaugh N S, Swain D L and Touma D 2015 Anthropogenic warming has increased drought risk in California *Proc. Natl Acad. Sci.* **112** 3931–6
Dong B and Dai A 2015 The influence of the interdecadal Pacific oscillation on temperature and precipitation over the globe *Clim. Dyn.* **45** 2667–81
Dong B, Dai A, Vuille M and Timm O E 2018 Asymmetric modulation of ENSO teleconnections by the interdecadal Pacific oscillation *J. Clim.* **31** 7337–61
Dunn R J, Hurst D F, Gobron N and Willett K M 2017 Global climate [in 'State of the Climate in 2016'] *Bull. Am. Meteorol. Soc.* **98** 5–62
Florenchie P, Lutjeharms J R, Reason C, Masson S and Rouault M 2003 The source of Benguela Niños in the South Atlantic Ocean *Geophys. Res. Lett.* **30** 1505
García-Herrera R, Garrido-Perez J M, Barriopedro D, Ordóñez C, Vicente-Serrano S M, Nieto R, Gimeno L, Sorí R and Yiou P 2019 The European 2016/17 drought *J. Clim.* **32** 3169–87
Gelaro R, Mccarty W, Suárez M J, Todling R, Molod A, Takacs L, Randles C A, Darmenov A, Bosilovich M G and Reichle R 2017 The Modern-Era Retrospective Analysis for Research and Applications, version 2 (MERRA-2) *J. Clim.* **30** 5419–54
Gibson P B, Waliser D E, Guan B, Deflorio M J, Ralph F M and Swain D L 2019 Ridging associated with drought across the Western and Southwestern United States: characteristics, trends and predictability sources *J. Clim.* **33** 2485-508

Hanel M, Rakovec O, Markonis Y, Máca P, Samaniego L, Kyselý J and Kumar R 2018 Revisiting the recent European droughts from a long-term perspective *Sci. Rep.* **8** 1–11
Harris I, Osborn T J, Jones P and Lister D 2020 Version 4 of the CRU TS monthly high-resolution gridded multivariate climate dataset *Sci. Data.* **7** 109
Hendon H H 2003 Indonesian rainfall variability: impacts of ENSO and local air–sea interaction *J. Clim.* **16** 1775–90
Herrera-Estrada J E, Martinez J A, Dominguez F, Findell K L, Wood E F and Sheffield J 2019 Reduced moisture transport linked to drought propagation across North America *Geophys. Res. Lett.* **46** 5243–53
Hersbach H 2016 The ERA5 Atmospheric Reanalysis AGU fall meeting abstracts
Hill K J, Taschetto A S and England M H 2009 South American rainfall impacts associated with inter-El Niño variations *Geophys. Res. Lett.* **36** L19702
Hoerling M and Kumar A 2003 The perfect ocean for drought *Science* **299** 691–4
Hong C, Hsu H, Lin N and Chiu H 2011 Roles of European blocking and tropical-extratropical interaction in the 2010 Pakistan flooding *Geophys. Res. Lett.* **38** L13806
Kao H-Y and Yu J-Y 2009 Contrasting eastern-Pacific and central-Pacific types of ENSO *J. Clim.* **22** 615–32
Karl T R 1986 The sensitivity of the Palmer Drought Severity Index and Palmer's Z-index to their calibration coefficients including potential evapotranspiration *J. Clim. Appl. Meteorol.* **25** 77–86
Kornhuber K, Osprey S, Coumou D, Petri S, Petoukhov V, Rahmstorf S and Gray L 2019 Extreme weather events in early summer 2018 connected by a recurrent hemispheric wave-7 pattern *Environ. Res. Lett.* **14** 054002
Kosaka Y and Xie S-P 2013 Recent global-warming hiatus tied to equatorial Pacific surface cooling *Nature* **501** 403–7
Kripalani R H and Singh S V 1993 Large scale aspects of India-China summer monsoon rainfall *Adv. Atmos. Sci.* **10** 71–84
Lau W K and Kim K-M 2012 The 2010 Pakistan flood and Russian heat wave: teleconnection of hydrometeorological extremes *J. Hydrometeorol.* **13** 392–403
Lee H and Zhang D 2011 Relationship between NAO and drought disasters in northwestern China in the last millennium *J. Arid Environ.* **75** 1114–20
Lesk C, Rowhani P and Ramankutty N 2016 Influence of extreme weather disasters on global crop production *Nature* **529** 84–87
Liebmann B and Smith C A 1996 Description of a complete (interpolated) outgoing longwave radiation dataset *Bull. Am. Meteorol. Soc.* **77** 1275–7
Lund J, Medellin-Azuara J, Durand J and Stone K 2018 Lessons from California's 2012–2016 drought *J. Water Resour. Plann. Manage.* **144** 04018067
Luo L, Apps D, Arcand S, Xu H, Pan M and Hoerling M 2017 Contribution of temperature and precipitation anomalies to the California drought during 2012–2015 *Geophys. Res. Lett.* **44** 3184–92
Masih I, Maskey S, Mussá F and Trambauer P 2014 A review of droughts on the African continent: a geospatial and long-term perspective *Hydrol. Earth Syst. Sci.* **18** 3635
Mccabe G J, Palecki M A and Betancourt J L 2004 Pacific and Atlantic Ocean influences on multidecadal drought frequency in the United States *Proc. Natl Acad. Sci.* **101** 4136–41
Miralles D G, Gentine P, Seneviratne S I and Teuling A J 2019 Land–atmospheric feedbacks during droughts and heatwaves: state of the science and current challenges *Ann. N. Y. Acad. Sci.* **1436** 19
Munday C and Washington R 2017 Circulation controls on southern African precipitation in coupled models: the role of the Angola low *J. Geophys. Res. Atmos.* **122** 861–77
Nakamura H, Nakamura M and Anderson J L 1997 The role of high-and low-frequency dynamics in blocking formation *Mon. Weather Rev.* **125** 2074–93
Nguyen P-L, Min S-K and Kim Y-H 2020 Combined impacts of the El Niño-Southern Oscillation and Pacific Decadal Oscillation on global droughts assessed using the standardized precipitation evapotranspiration index *Int. J. Climatol.*
Okin G S, Dong C, Willis K S, Gillespie T W and Macdonald G M 2018 The impact of drought on native southern California vegetation: remote sensing analysis using MODIS-derived time series *J. Geophys. Res. Biogeosci.* **123** 1927–39
Palmer W C 1965 Meteorological Drought *US Weather Bureau Research Paper* **45** 1 58
Pomposi C, Funk C, Shukla S, Harrison L and Magadzire T 2018 Distinguishing southern Africa precipitation response by strength of El Niño events and implications for decision-making *Environ. Res. Lett.* **13** 074015
Ropelewski C and Folland C 2000 Prospects for the prediction of meteorological drought *Drought Glob. Assess.* **1** 21–40
Seager R and Henderson N 2016 On the role of tropical ocean forcing of the persistent North American West Coast ridge of winter 2013/14 *J. Clim.* **29** 8027–49
Seager R, Hoerling M, Schubert S, Wang H, Lyon B, Kumar A, Nakamura J and Henderson N 2015 Causes of the 2011–14 California drought *J. Clim.* **28** 6997–7024
Service (C3S) CCC 2017 *ERA5: Fifth generation of ECMWF atmospheric reanalyses of the global climate, Copernicus Climate Change Service Climate Data Store (CDS)*
Shen C, Wang W-C, Hao Z and Gong W 2007 Exceptional drought events over eastern China during the last five centuries *Clim. Change* **85** 453–71
Simpkins G 2018 Running dry *Nat. Clim. Change* **8** 369–369
Su B, Huang J, Fischer T, Wang Y, Kundzewicz Z W, Zhai J, Sun H, Wang A, Zeng X and Wang G 2018 Drought losses in China might double between the 1.5 C and 2.0 C warming *Proc. Natl Acad. Sci.* **115** 10600–5
Swain D L, Horton D E, Singh D and Diffenbaugh N S 2016 Trends in atmospheric patterns conducive to seasonal precipitation and temperature extremes in California *Sci. Adv.* **2** e1501344
Swain D L, Singh D, Horton D E, Mankin J S, Ballard T C and Diffenbaugh N S 2017 Remote linkages to anomalous winter atmospheric ridging over the northeastern Pacific *J. Geophys. Res. Atmos.* **122** 12,194–12,209
Tan X, Bao M, Hartmann D L and Ceppi P 2017 The role of synoptic waves in the formation and maintenance of the Western Hemisphere circulation pattern *J. Clim.* **30** 10259–74
Trenberth K, Jones P, Ambenje P, Bojariu R, Easterling D, Tank A K, Parker D, Rahimzadeh F, Renwick J and Rusticucci M 2007 Observations: surface and atmospheric climate change (Cambridge: Cambridge University Press) Chapter 3 235–336 (https://www.ipcc.ch/report/ar4/wg1/)
Ummenhofer C C, England M H, Mcintosh P C, Meyers G A, Pook M J, Risbey J S, Gupta A S and Taschetto A S 2009 What causes southeast Australia's worst droughts? *Geophys. Res. Lett.* **36** L04706
van der Schrier G, Barichivich J, Briffa K and Jones P 2013 A scPDSI-based global data set of dry and wet spells for 1901–2009 *J. Geophys. Res. Atmos.* **118** 4025–48
Vicente-Serrano S M, López-Moreno J I, Gimeno L, Nieto R, Morán-Tejeda E, Lorenzo-Lacruz J, Beguería S and Azorin-Molina C 2011 A multiscalar global evaluation of the impact of ENSO on droughts *J. Geophys. Res. Atmos.* **116** D20109
Wallace J M and Gutzler D S 1981 Teleconnections in the geopotential height field during the Northern Hemisphere winter *Mon. Weather Rev.* **109** 784–812
Wang L, Chen W and Huang R 2008 Interdecadal modulation of PDO on the impact of ENSO on the east Asian winter monsoon *Geophys. Res. Lett.* **35** L20702

Wang S-Y, Hipps L, Gillies R R and Yoon J-H 2014a Probable causes of the abnormal ridge accompanying the 2013–2014 California drought: ENSO precursor and anthropogenic warming footprint *Geophys. Res. Lett.* **41** 3220–6

Wang S, Huang J, He Y and Guan Y 2014b Combined effects of the Pacific decadal oscillation and El Nino-Southern oscillation on global land dry–wet changes *Sci. Rep.* **4** 6651

Wang X and Liu H 2016 PDO modulation of ENSO effect on tropical cyclone rapid intensification in the western North Pacific *Clim. Dyn.* **46** 15–28

Webb R, Rosenzweig C E and Levine E R 2000 Global soil texture and derived water-holding capacities (Webb et al) (*Ornl Daac*)

Wise E K 2016 Five centuries of US West Coast drought: occurrence, spatial distribution, and associated atmospheric circulation patterns *Geophys. Res. Lett.* **43** 4539–46

Wolf G, Brayshaw D J, Klingaman N P and Czaja A 2018 Quasi-stationary waves and their impact on European weather and extreme events *Q. J. R. Meteorol. Soc.* **144** 2431–48

Wolski P 2018 How severe is Cape Town's 'Day Zero' drought? *Significance* **15** 24–27

Xu C, Mcdowell N G, Fisher R A, Wei L, Sevanto S, Christoffersen B O, Weng E and Middleton R S 2019 Increasing impacts of extreme droughts on vegetation productivity under climate change *Nat. Clim. Change* **9** 948–53

Yang S, Li Z, Yu J-Y, Hu X, Dong W and He S 2018a El Niño–Southern Oscillation and its impact in the changing climate *Natl Sci. Rev.* **5** 840–57

Yang Y, Saatchi S S, Xu L, Yu Y, Choi S, Phillips N, Kennedy R, Keller M, Knyazikhin Y and Myneni R B 2018b Post-drought decline of the Amazon carbon sink *Nat. Commun.* **9** 1–9